Available online at www.sciencedirect.com
SCIENCE DIRECT®
Polymer 44 (2003) 3515–3522
polymer
www.elsevier.com/locate/polymer

Structure and properties of poly(vinyl alcohol)/tungsten trioxide hybrids

Shoichiro Yano[a,*], Kimio Kurita[a], Keisuke Iwata[a], Takeshi Furukawa[b], Mitsuo Kodomari[b]

[a]*College of Science and Technology, Nihon University, 1-8-14 Kanda-surugadai, Chiyoda-ku, Tokyo 101-8303, Japan*
[b]*Shibaura Institute of Technology, 3-3-14 Shibaura, Minato-ku, Tokyo 108, Japan*

Received 18 September 2002; received in revised form 10 March 2003; accepted 31 March 2003

Abstract

PVA/WO_3 hybrids were produced by using ion exchange process of $Na_2WO_4{\cdot}2H_2O$. Microstructures of this hybrid was estimated by SAXS measurement as follows; the WO_3 rich domains having radius of gyration of about 5.7 nm (estimated in Guinier regime), in which PVA chains were partly incorporated, were dispersed evenly in PVA matrix with the correlation length of 20–30 nm (approximated by Bragg equation). The electron density difference between WO_3 and matrix, $\Delta\rho$, was rather high and sharp, and this indicates that the domains dispersed in PVA matrix is rich in WO_3 component. The physical properties of the hybrids were affected by the morphology. The mechanical properties of the hybrid were improved markedly, e.g. the tensile strength increased from 35 MPa (PVA) to 55 MPa at 27 wt% of WO_3 content, and the modulus also increased above T_g with increasing amount of WO_3. A tan δ peak appeared at 75 °C shifted to the higher temperature side with WO_3 content. These were caused by strong interaction between PVA chains and WO_3 domains, which was formed by incorporation of PVA chain into WO_3 domains having hydrogen bonding. This hybrid was transparent and showed the photochromism especially at low concentration of WO_3. When UV–visible light of wavelength above 350 nm was irradiated on the hybrid, a minimum occurred at 630 nm in the UV–visible spectrum, and color changed from yellow to blue. Bleaching occurred in the dark in 100% relative humidity. Consequently, the ion exchange process was suitable to obtain PVA/WO_3 hybrid, since this procedure was simple and economical, and hybrid thus produced had excellent mechanical and photochromism properties.

Keywords: PVA/WO_3 hybrids; Microstructure; Mechanical properties

1. Introduction

Recently, attention has been paid to sol–gel derived organic–inorganic hybrids having nano-ordered disperse phase. The organic–inorganic hybrids having combined characteristics of organic polymers and inorganic substances promise new high performance or high functional materials [1–4].

The sol–gel process is usually carried out by hydrolysis and polycondensation reactions of metal alkoxides $M(OR)_n$, where M is Na, Ba, Ca, Cu, Al, Si, Ti, Ge, V, W, Y, etc. and R is CH_3, C_2H_5, C_3H_7, C_4H_9, etc. Various combinations of M and R are possible. In the sol–gel process, metal alkoxide, $M(OR)_n$ solution is hydrolyzed to form metal hydroxide, $M(OH)_n$ sol, which is reactive and converted to metal oxide gel. The sol–gel process proceeds at low temperature, and hence thermally unstable organic polymers can be incorporated with inorganic substances by the sol–gel process involving metal alkoxides [5,6].

We have studied preparation and properties of the various sol–gel derived organic–inorganic hybrids by using tetraethoxysilane (TEOS) and organic polymers such as poly(vinyl acetate) [7,8], hydroxypropyl cellulose [9,10], poly(vinyl alcohol) (PVA) [11], poly(vinylidene fluoride) [12], polypropyleneglycol (PPG) [13], and poly(ethyl acrylate) [14]. The mechanical properties of these organic polymers were improved markedly by incorporation of silica.

Preparation procedures of the sol–gel derived hybrids have been classified into three categories. (1) Mixing type; organic polymers are mixed with metal alkoxides followed by the sol–gel reactions [9–12], (2) Copolymer type; vinyl monomers are copolymerized with vinyltriethoxysilane or 3-methacryloxypropyltriethoxysilane, then mixed with metal alkoxides [7,8,14], and (3) End-cap type; ethoxysilyl groups are introduced on organic polymers by reacting isocyanatopropyltriethoxysilane with –OH or $-NH_2$ end

* Corresponding author. Tel./fax: +81-3-3259-0799.
E-mail address: yano@chem.cst.nihon-u.ac.jp (S. Yano).

0032-3861/03/$ - see front matter © 2003 Elsevier Science Ltd. All rights reserved.
doi:10.1016/S0032-3861(03)00281-7

groups of organic polymers prior to the sol–gel reactions with metal alkoxides [5,6]. In mixing type (1), hydrogen bonding plays an important role in compatibility between inorganic phase and polymer matrix, while in copolymer type (2) and end-cap type (3), covalent bonding is formed between inorganic phase and organic polymer [6]. The microstructure of the hybrid from type (1) (hydrogen bonding type) is different from types (2) and (3) (covalent bonding type). The SAXS pattern of the former type has no maximum and perhaps networks of inorganic phase are formed in organic polymer matrix. On the other hand, in the latter case, a sharp peak appeared in the SAXS profiles, and inorganic domains are formed in organic polymer matrix [6].

Inorganic materials have superior optical properties such as refractive index, transparency, and non-linear optics. Various optical materials made of organic–inorganic hybrids have been attempted. Wang and Wilkes [15] produced poly(tetramethylene oxide) (PTMO)/TiO_2 and PTMO/ZrO_2 hybrids having high refractive indexes of 1.65 at 60 wt% of TiO_2 content and 1.52 at 60 wt% of ZrO_2. We have also shown that PTMO/TiO_2 hybrid has high refractive index of 1.57 at 26 wt% of TiO_2 content, and this material effectively cut ultraviolet (UV) rays below 400 nm [16].

Transparent materials have been produced by mixing polymethyl methacrylate (PMMA) with TEOS in tetrahydrofuran, and morphology of the hybrids have been studied [17,18]. Transparent PMMA/silica composites have been also prepared by impregnation of MMA monomer into porous silica and polymerization in situ in the micro pores [19,20]. Philipp and Schmidt [21,22], have developed hard contact lenses by the sol–gel process of an epoxide substituted alkoxysilane and titaniumalkoxide.

Non-linear optical materials have been also produced by the sol–gel process. Prasad and his coworkers [23–26] have developed the third order non-linear optical materials composed of poly(*p*-phenylene vinylene), and SiO_2 or V_2O_5.

It is known that oxides of transition metals such as amorphous tungsten trioxide (WO_3) exhibit photochromism and electrochromism with the formation of tungsten bronze. The photochromism of WO_3 is enhanced in the presence of organic polymers containing OH groups [27]. When protons and electrons are injected into WO_3, intervalence electron transfer between W^{5+} and W^{6+} occurs, and tungsten bronze is formed. OH groups in organic polymers are considered to be a source of protons

$$WO_3 + xH^+ + xe^- \rightarrow H_xWO_3(\text{tungsten bronze})$$

Kuboyama et al. [27,28] have prepared poly(ethylene glycol)(PEG)/WO_3 hybrid and studied the photochromic properties of this hybrid. We have also prepared PEG/WO_3 [29] and PTMO/WO_3 [30], and have studied the photochromism and mechanical properties. In these cases, origomers with molecular weight less than 1000 have been used, and the hybrids have had low T_gs and poor mechanical properties, even though excellent photochromism has been shown.

WO_3 can be prepared by two kinds of procedures; one is the ion exchange process of sodium tungstate dihydrate ($Na_2WO_4{\cdot}2H_2O$) and the other is the sol–gel process involving tungsten hexaethoxide [$W(OC_2H_5)_6$]. The hybrid prepared by the sol–gel process of tungsten alkoxide had poor mechanical properties and was opaque, because of deposition of insoluble part of the alkoxide [31]. In this study, therefore, ion exchange process of $Na_2WO_4{\cdot}2H_2O$ is employed, which is categorized in the type (1) process. Since this process is water system, hydrophilic polymers should be used. Here, we use PVA to prepare mechanically strong, free standing, and transparent WO_3 hybrid films. The morphology of the hybrids prepared by the ion exchange process has not been studied, but may be different from that of the hybrid derived from the sol–gel process involving metal alkoxides. In this work, the thermal, mechanical, and photochromic properties of the PVA/WO_3 hybrid are studied correlated with microstructure evaluated by SAXS.

2. Experimental

2.1. Materials

PVA used for this study was purchased from Scientific Polymer Products. The molecular weight was 10,000, and degree of saponification was 88%. Sodium tungstate (VI) dihydrate ($Na_2WO_4{\cdot}2H_2O$) was supplied by Kanto Chemicals Co., Inc. H-type ion exchange resin 50W-X20 was purchased from Dow Chemical Co.

Ion exchange resin was conditioned as follows; 50 g of the resin was immersed in sufficient amounts of water and the swollen resin was packed in a column with 300 mm length and 20 mm diameter. H-type resin was converted to Na-type resin by passing 500 ml of 1N aqueous solution of sodium chloride. Subsequently, the resin was recovered to H-type again by passing 1000 ml of 2N aqueous solution of hydrochloric acid. This procedure was repeated twice, and then passed 1000 ml of water in order to remove excess HCl in the column.

When 14.2 wt% aqueous solution of sodium tungstate (VI) dihydrate ($Na_2WO_4{\cdot}2H_2O$) passed through the column filled with conditioned H-type ion exchange resin, 10 wt% H_2WO_4 aqueous solution was obtained. Before gelation occurred 5 wt% PVA aqueous solution was mixed with the 10 wt% H_2WO_4 aqueous solution. The mixture was transferred into a Petri dish and was allowed to stand at room temperature for a week. After evaporation of water at 50 °C for a week in vacuo, yellowish transparent hybrid films were obtained. Content of WO_3 in PVA matrix was

controlled by adding amount of H_2WO_4 solution:

$$Na_2WO_4{\cdot}2H_2O \xrightarrow{\text{Ion exchange resin}} H_2WO_4 \xrightarrow{-H_2O} WO_3$$

2.2. Measurements

The thermogravimetry (TG) was made using a Seiko TG/DTA 320 (Seiko Instruments Inc.) at a heating rate of 10 °C/min in air. Evolved gasses during the TG measurements were detected by using the TG apparatus equipped with a mass spectrometer (MAC Science, Inc.). The mass numbers of the evolved gasses were determined by a histogram scan method between the mass number 10 and 100 at the temperatures where the decrease in the weight of sample occurred. After the mass numbers were determined, the mass spectra were recorded by using the multiple ion monitoring method during the TG measurements.

Wide angle X-ray diffraction was measured by using a Rigaku vertical type diffractometer equipped with a scintillation counter at scanning rate of 1°/min. Ni filtered Cu Kα X-ray beam was generated at 50 kV and 250 mA.

Small-angle X-ray scattering (SAXS) measurements were performed using an Anton Paar compact Kratky camera equipped with a scintillation counter. The camera length was 210 mm, the entrance slit was 40 mm, and the counter slit was 100 mm. The correction of the slit was done by the Glatter method [32]. All profiles were desmeared for the effects of slit collimation of the Kratky camera. An X-ray generator used was a Rigaku RINT-2500 V, and was operated at 50 kV and 250 mA. Ni filtered Cu Kα beam was used.

Tensile properties were measured on an Instron universal testing instrument TM-M (Instron Engineering Co.) at 25 °C and 50% relative humidity. The rectangular specimens with 5 mm wide and about 0.1 mm thick were tested at a constant crosshead speed of 10 mm/min with a gauge length of 10 mm.

The dynamic viscoelastic properties were measured using a dynamic viscoelastic analyzer (IT Keisoku Co. DVA-200) at a frequency of 10 Hz. The dynamic modulus, E' and tan δ were measured as a function of temperature. The heating rate was 2 °C/min.

Ultraviolet–visible light spectra were taken with a UV–VIS RECORDING SPECTRO-PHOTOMETER UV-25OOPC (Shimadzu) for PVA/WO_3 hybrids before and after ultraviolet light irradiation with 500 W xenon lamp ($\lambda \geq 350$ nm) with an UV35 filter.

3. Results and discussion

3.1. Thermo gravimetry (TG)

Fig. 1 shows the thermo gravimetry (TG) of the hybrids in air as a function of WO_3 content. In this TG curves several steps are observed as indicated by arrows. Temperature at each step is listed in Table 1. WO_3 content is calculated from the residual weight in TG curves at 800 °C. However, as is very difficult to control absorbed water content in the hybrids, this WO_3 content is only approximate value. The first step at about 90 °C is due to desorption of water in the hybrids. The second step from 160 to 280 °C may be due to the dehydration reaction of –OH groups in PVA chains. This temperature shifts to the lower temperature side, if the WO_3 content increases. This behavior is also observed in PVA/SiO_2 system [11]. The dehydration reaction of PVA is accelerated by inorganic component in the hybrid, which may act as catalyst for dehydration reaction. The third and fourth steps in the TG curves are caused by the degradation of PVA matrix releasing CO_2 gas. The forth step occurs at about 500 °C depending on the content of WO_3, and shifts to the higher temperature when WO_3 content increases. This may be caused by evaporation of CO_2 originated from organic compounds strongly adsorbed on WO_3 phase.

The evolved gases during TG measurements are analyzed by using a TG/MASS apparatus as shown in Fig. 2. Fig. 2(A) shows the TG/MASS curves of PVA in air. During TG measurement, PVA releases H_2O at about 115 °C by desorption, and at 355, 440, and 480 °C by dehydration reaction of PVA. CO_2 is released at 355, 440, and 480 °C by degradation of PVA. Very small amounts of other gasses are admitted but can not be recorded at the same level of H_2O and CO_2. TG/MASS curves of PVA/WO_3 (45 wt%) hybrid in air are shown in Fig. 2(B). H_2O is released at 100, 200 and 410 °C by desorption and dehydration. CO_2 is also detected at 410, 430, and 487 °C, but is not found at 355 °C which appears in the spectrum of PVA.

3.2. Microstructure of PVA/WO_3 hybrids

Fig. 3 shows wide angle X-ray scattering (WAXS) patterns of PVA, PVA/WO_3 hybrids, and WO_3 made by the ion exchange process. PVA the crystalline polymer exhibits peaks at $\theta = 20°$ and 40°, but the crystallization is restricted

Table 1
Onset temperatures at stepwise changes in the weight of PVA/WO_3 hybrids prepared by the ion exchange process

WO_3 content (wt%)	Onset temperatures (°C)			
	First step	Second step	Third step	Fourth step
0	90	280	400	460
8	90	270	410	510
15	90	250	410	500
25	90	210	410	510
27	90	180	400	550
37	90	160	380	600

WO_3 content is calculated by the residual weight in TG curve at 800 °C.

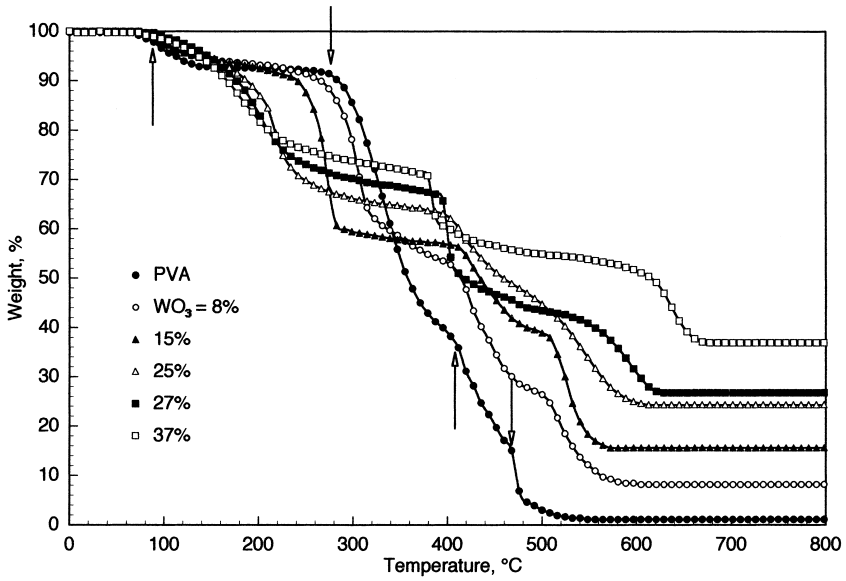

Fig. 1. TG curves for PVA/WO_3 hybrids as a function of WO_3 content in air.

during formation of hybrids containing WO_3 above 25 wt%. Bulk WO_3 prepared by the ion exchange process shows crystalline peaks. It is interesting that WO_3 which shows crystalline peaks in the bulk state does not show these peaks but shows amorphous pattern (Fig. 3) in the hybrids. This may be interpreted that WO_3 in the hybrids are dispersed homogeneously in PVA matrix as nano-ordered fine particles.

The morphology of the PVA/WO_3 hybrids is also studied by using small angle X-ray scattering method (SAXS). The SAXS technique provides supplemental information about average particle size or correlation length, the organic–inorganic phase boundary, and the degree of ramification of the inorganic phase. Fig. 4 shows SAXS profiles of the PVA/WO_3 hybrids as a function of WO_3 content. Intensity $I(q)$ is plotted against scattering wave vector q [$= (4\pi/\lambda)\sin(\theta/2)$], where λ is the wavelength of X-ray, i.e. 0.154 nm, and θ is the scattering angle. In the SAXS profile of PVA, a peak appears at $q = 0.6\ \mathrm{nm}^{-1}$ which is caused by the long period of PVA crystallites. In the SAXS profiles of PVA/WO_3 hybrids, the peak at $q = 0.6\ \mathrm{nm}^{-1}$ disappears above 25 wt% of WO_3 content. This is caused by the restriction of PVA crystallization with increasing WO_3 content. A small and broad peak appears at about $q_{max} = 0.2–0.3\ \mathrm{nm}^{-1}$ above 15 wt% of WO_3. This may be due to the interference among WO_3 domains. The correlation length d can be approximated as 20–30 nm by using Bragg's equation (1).

$$d = 2\pi/q_{max} \tag{1}$$

It is known that the Porod equation (2) holds for the middle q region in the SAXS profiles

$$I(q) \propto q^{-D} \tag{2}$$

where D is the power law exponent and is correlated with fractal dimension. Schaefer [33,34] has shown the morphology of various sol–gel derived ceramics such that $D = 4$ for smooth surface colloids, $D = 3$ for rough surface colloids, and $D = 1.9–2.5$ for branched three-dimensional networks. Using the data from Fig. 4, D is calculated as 1.8 for 15 wt% of WO_3 and 1.9 for 25–37 wt% of WO_3. WO_3 perhaps forms network in the domain.

Dimension of the WO_3 domain is evaluated by using Guinier's equation (3) at the smaller scattering angle region

$$I(q) = I(0)\exp(-q^2R_g^2/3) \tag{3}$$

where $I(0)$ is the intensity at $q = 0$, and R_g the radius of gyration. R_g at low volume fraction v_f of WO_3, can be evaluated as 4.6 nm at 8 wt% ($v_f = 1.6$ vol%), and 6.7 nm at 15 wt% ($v_f = 3.2$ vol%). At lower volume fraction of WO_3 than 3.2 vol%, average about 5.7 nm of WO_3 domains may disperse homogeneously with correlation length of 20–30 nm in PVA matrix. The volume fraction is calculated by using densities of WO_3 (7.29 g/cm^3) and PVA (1.35 g/cm^3).

A broad peak appears at about $q = 3–4\ \mathrm{nm}^{-1}$, which is caused by interference between WO_3 domains dispersed in PVA matrix. This peak can be also observed in PTMO/WO_3 [30] and PEG/WO_3 hybrid [35].

In order to evaluate the microphase segregation of inorganic dispersant from polymer matrix, the mean square electron density fluctuation can be used. The actual mean square electron density fluctuation, $\langle\eta^2\rangle_{obs}$, for an isotropic sample can be calculated according to

$$\langle\eta^2\rangle_{obs} = \frac{1}{2\pi^2}\int_0^\infty q^2 I(q)\,\mathrm{d}q = \frac{Q}{2\pi^2} \tag{4}$$

where Q is the invariant defined by Porod [36]. The ideal mean square electron density fluctuation, $\langle\eta^2\rangle_{cal}$, is calculated under the assumption of complete segregation

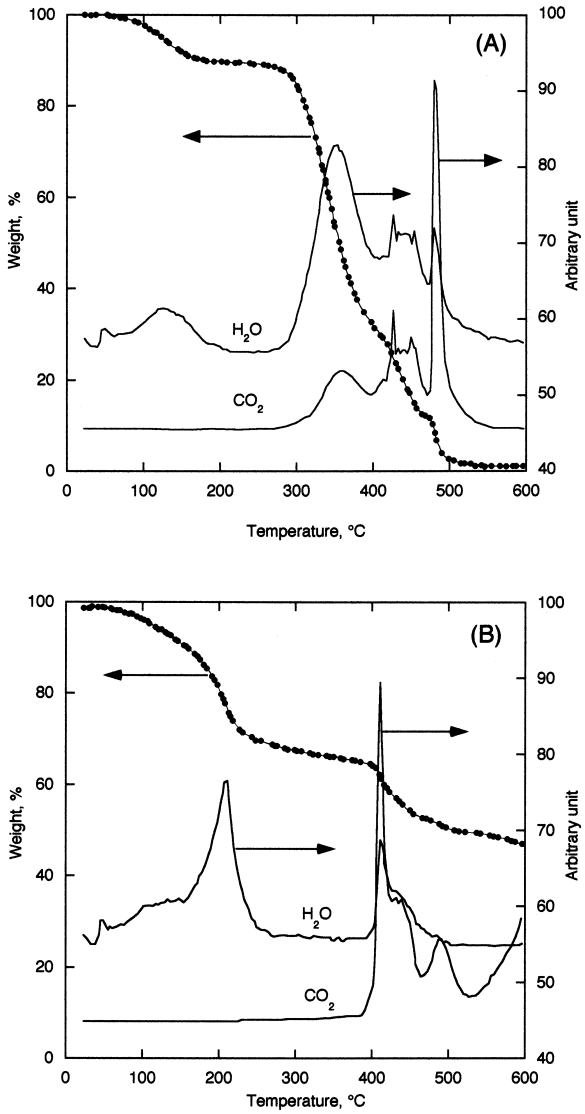

Fig. 2. TG/MASS curves for (A) PVA and (B) PVA/WO_3 hybrid (WO_3 content 45%) in air.

and sharp domain boundaries as expressed in Eq. (5)

$$\langle\eta^2\rangle_{cal} = \phi_A(1-\phi_A)(\Delta\rho)^2 \cong v_f(1-v_f)(\Delta\rho)^2 \quad (5)$$

where $\Delta\rho$ is the electron density difference, and ϕ_A is volume fraction of the WO_3 domain phase but is difficult to evaluate, since the WO_3 domain is mixed with PVA chains. Therefore, ϕ_A can be approximated by the volume fraction of WO_3 content, v_f. The degree of microphase segregation, DS, can be defined by Eq. (6)

$$DS = [\langle\eta^2\rangle_{obs}/\langle\eta^2\rangle_{cal}]^{1/2} \quad (6)$$

DS is plotted against v_f in Fig. 5. The values of DS for the PVA/ion exchanged WO_3 hybrids are almost constant about 0.56. The microstructure of the hybrid deviates from the ideal state (DS = 1), i.e. complete microphase segregation occurs with rather sharp domain boundaries. However, in PVA/ion exchanged WO_3 hybrids, microphase segregation

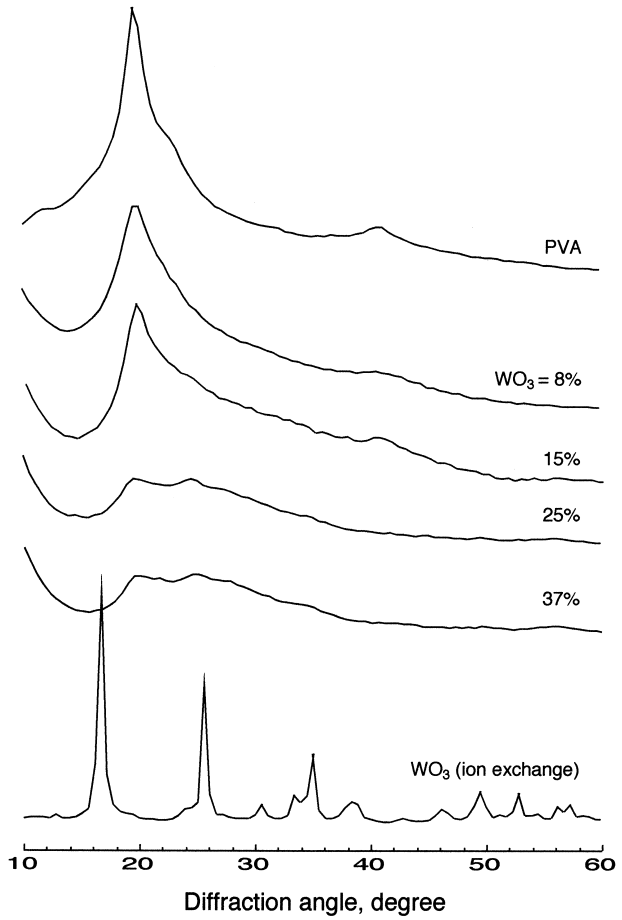

Fig. 3. X-ray diffraction patterns for WO_3, PVA, and PVA/WO_3 hybrids prepared by ion exchange process.

occurs to some extent, and WO_3 rich domains may be formed; in this domain PVA chains are partly incorporated.

From the WAXS and SAXS results described above, possible morphology of the PVA/WO_3 hybrids is estimated. Fig. 6 shows the morphological model for the hybrid prepared by the ion exchange process. WO_3 rich domains having R_g of about 5.7 nm disperse in PVA matrix homogeneously with the correlation length of 20–30 nm. In the vicinity of interface of the domain, some PVA chains are incorporated. This domain is composed of WO_3 networks. The electron density difference, $\Delta\rho$ is high and sharp.

3.3. Mechanical properties

3.3.1. Stress–strain curves

Fig. 7 shows the stress–strain curves of the PVA/WO_3 hybrids prepared by the ion exchange process as a function of WO_3 content. The elongation decreases with increasing amounts of WO_3, but the tensile stress and ultimate strength significantly increase with increasing content of WO_3. The yield stress is still observed in the hybrid containing 37 wt% of WO_3. As can be seen in Fig. 6, PVA chains incorporated in the WO_3 rich domains, and hydrogen bonding between

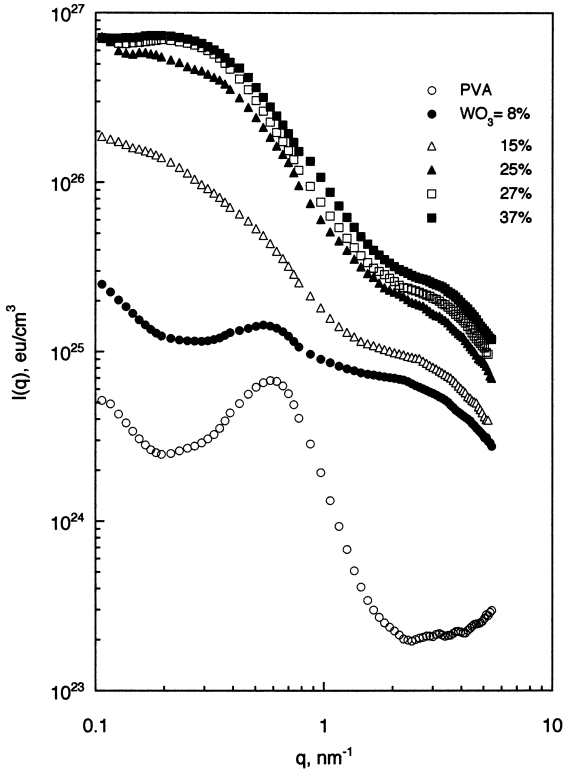

Fig. 4. Small angle X-ray scattering for PVA/WO_3 hybrids as a function of WO_3 content.

PVA chains and WO_3 improve the mechanical properties of the hybrids.

3.3.2. Dynamic viscoelasticity

Fig. 8 shows the temperature dependence of the dynamic viscoelastic properties of the PVA/WO_3 hybrid. As can be seen in this figure, the dynamic modulus, E', is improved with loading amount of WO_3 above glass transition temperature (T_g). This is caused by the effect of mixing

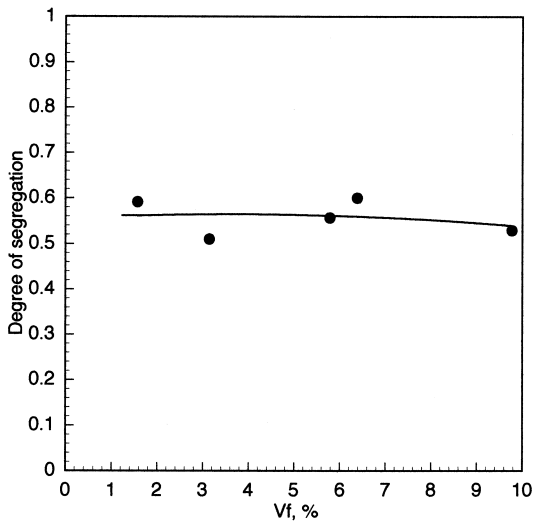

Fig. 5. Plots of degree of segregation, DS versus volume fraction v_f of WO_3 in the hybrids.

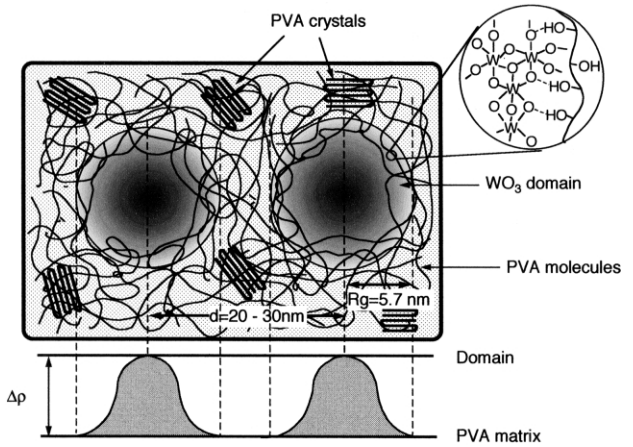

Fig. 6. Morphological models for PVA/WO_3 hybrid prepared by ion exchange process.

the high modulus component (WO_3), and the strong interaction between WO_3 and PVA as described above. Temperature dependence of E' of the hybrids rises at 170, 130, and 120 °C when the WO_3 content changes as 15, 27, and 37 wt%, respectively. This rise in E' may be due to the dehydration reaction of OH groups in PVA matrix corresponding to the TG curves below 200 °C (see Figs. 1 and 2), and is enhanced by the existence of inorganic component, WO_3.

In the tan δ curve of PVA, a large peak appears at 75 °C, which is attributed to the glass transition of PVA. PVA/WO_3 hybrid has a shoulder peak at the lower temperature side of the main tan δ peak, whose position depends on the WO_3 content, i.e. 95, 100, and 110 °C for PVA loaded with 15, 27, and 37% of WO_3, respectively. The shoulder peak may be due to desorption of residual solvent (water) from the hybrid. The position of the large main peak also depends on the WO_3 content and appears at 105, 130, and 135 °C for the hybrids containing 15, 27, and 37% of WO_3, respectively. The main peak of the hybrid is caused by the micro-Brownian motion of PVA chains strongly restricted by the dispersed WO_3 domains in the hybrid as depicted in Fig. 6.

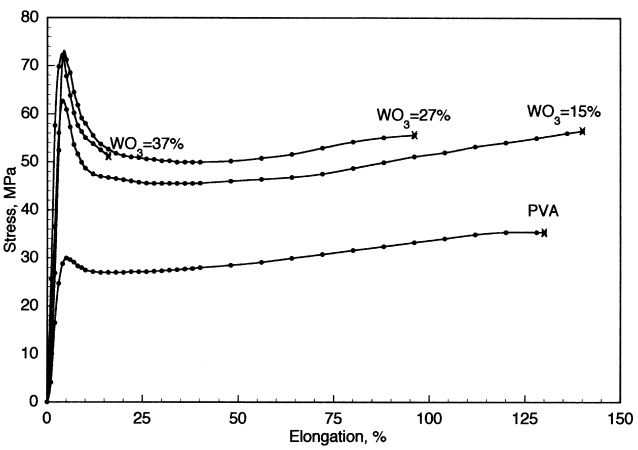

Fig. 7. Stress–strain curves for PVA and PVA/WO_3 hybrids as a function of WO_3 content.

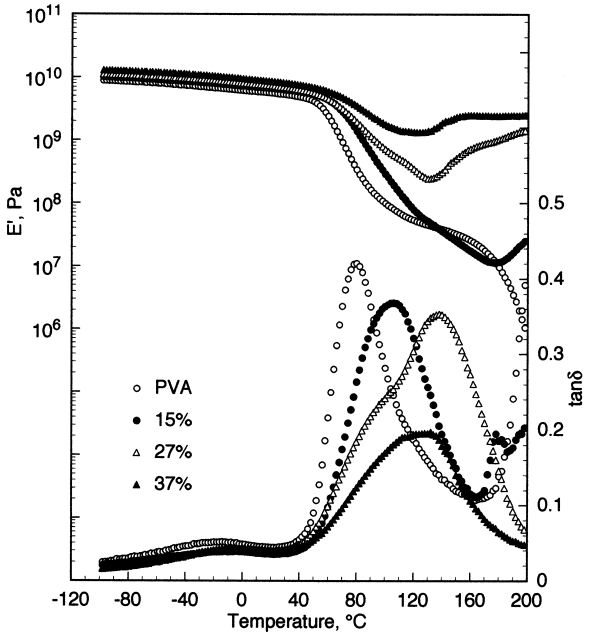

Fig. 8. Dynamic viscoelastic properties for PVA and PVA/WO_3 hybrids as a function of WO_3 content.

PVA chains may interact with dispersed WO_3 domains as described above. The intensity of the main peak decreases with increasing WO_3 content. The hybrid prepared by the ion exchange process is categorized in the type (1) process as described above. Usually, the tan δ peak position of the hybrids derived from the type (1) process does not shift to the higher temperature side because of weak interaction (hydrogen bonding) between inorganic phase and polymer matrix [9,11,12].

A low and broad tan δ peak is also observed at about -20 °C, which shift to higher temperature with increasing WO_3 content. This peak corresponds to the β-relaxation correlated to the absorbed water (water dispersion), which is frequently appears in hydrophilic polymers such as nylons [37–40] and PVA [41]. Origin of the β-relaxation is reported as the rotational motion of water molecules which are bound to hydrophilic groups by hydrogen bonds [37], or the motion of the water/polymer complex [39]. The β-peak of nylons appears at about -40 °C and that of PVA at -20 °C [41]. As is seen in Fig. 8, the β peak of the hybrids shifts to the higher temperature side, which is restricted by the induced domains.

3.3.3. UV visible spectrum

It is known that amorphous tungsten trioxide exhibits photochromism when ultraviolet rays are irradiated, and this photochromism is enhanced by the presence of polymer having OH groups [27,28]. Bulk WO_3 itself does not exhibit photochromism. Fig. 9 shows the UV–visible spectra of the PVA/WO_3 hybrids prepared by the ion exchange process before and after irradiation with UV light of wavelength

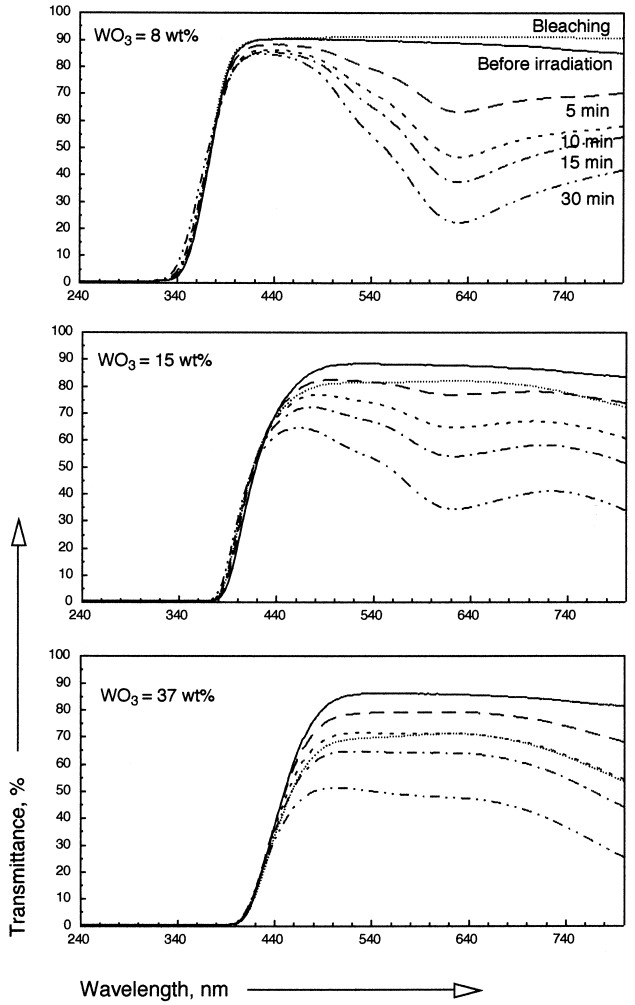

Fig. 9. UV–visible spectra for PVA/WO_3 hybrids prepared by ion exchange process.

above 350 nm. Thickness of the sample is about 50 μm and transmittance at 400–800 nm is about 80–90%. When UV light is irradiated on the sample, a minimum appears at about 630 nm in the UV–visible spectrum, which decreases with irradiation time, and color changes from pale yellow to blue, since amorphous WO_3 have changed to tungsten bronze structure. At 37 wt%, of WO_3, the minimum at about 630 nm does not appear clearly, but the transmittance level decreases over the wavelength range from 440 to 800 nm due to the increase in the concentration of WO_3. Color changes from yellow to dark blue. Bleaching of the irradiated sample hardly occurs in a dry state in the dark. However, when the sample placed in the dark at 100% relative humidity for 1 day, bleaching occurs as indicated by a dotted line in the figure, and color changed from blue to yellow. At 8 wt% of WO_3 bleaching occurs completely, but at 15 wt % and at 37 wt% insufficient bleaching occurs until 80 and 70%, respectively. As absorbed water in the hybrid samples may play an important role on photochromism, more study is required to make clear the mechanism [35].

References

[1] Klein Lc, editor. Sol–gel optics: processing and applications. Dordrecht: Kluwer Academic Publisher; 1994.
[2] Coltrain BK, Sanchez C, Schaefer DW, Wilkes GL, editors. Better ceramics through chemistry VII: organic/inorganic hybrid materials. Pittsburgh, Pennsylvania: Materials Research Society; 1996.
[3] Laine RM, Sanchez C, Brinker CJ, Giannelis E, editors. Organic/inorganic hybrid materials. Warrendale, Pennsylvania: Materials Research Society; 1998.
[4] Schmidt H, editor. Sol Gel production. Switzerland: Trans Tech Publications; 1998.
[5] Yano S, Iwata K, Kurita K. Mater Sci Engng 1998;C6:75.
[6] Kurita K, Yano S. Rep Prog Polym Phys Jpn 2000;43:689.
[7] Yano S, Nakamura K, Yamauchi N. J Appl Polym Sci 1994;54:163.
[8] Yano S, Furukawa T, Kodomari M. J Nat Inst Mater Chem Res 1996; 4:231.
[9] Yano S. Polymer 1994;25:5565.
[10] Yano S, Kodomari M. Nihon Reoroji Gakkaishi (J Soc Rheol Jpn) 1996;24:15.
[11] Yano S, Furukawa T, Kodomari M, Kurita K. Kobunshi Ronbunshu (Jpn J Polym Sci Technol) 1996;53:218.
[12] Yano S, Okubo N, Takahashi K. Macromol Symp 1996;108:279.
[13] Yano S, Iwata K, Kurita K, Sawaguchi T. Kobunshi Ronbunshu (Jpn J Polym Sci Technol) 2000;57:383.
[14] Saito T, Yano S, Sawaguchi T, Hashimoto W, Kurita K. Kobunshi Ronbunshu (Jpn J Polym Sci Technol) 2000;57:389.
[15] Wang B, Wilkes GL. J Polym Sci 1991;29:905.
[16] Hashimoto W, Kamiyama N, Kawai M, Naito M, Kurita K, Yano S. Polym Prepr Jpn 2000;49:2127.
[17] Silveira KF, Valeria I, Yoshida P, Nunes SP. Polymer 1995;36:1425.
[18] Landry CJT, Coltrain BK, Brady BK. Polymer 1992;33:1486.
[19] Pope EJA, Asami M, Mackenzie JD. J Mater Res 1989;4:1018.
[20] Abramoff R, Klein LC. In: Mackenzie JD, Ulrich DR, editors. Sol–gel optics. New York: SPIE; 1990. p. 241.
[21] Philipp G, Schmidt H. Non-Cryst Solids 1984;63:283.
[22] Schmidt H. Non-Cryst Solids 1989;112:419.
[23] Wung CJ, Pang Y, Prasad PN, Karaz FE. Polymer 1991;32:605.
[24] Prasad PN. Better ceramics through chemistry IV. Mater Res Soc Symp Proc 1990;180:741.
[25] Wung CJ, Lee KS, Prasad PN, Kim JC, Jin J-Il, Shim HK. Polymer 1992;33:4145.
[26] Wung CJ, Wijekoon WMKP, Prasad PN. Polymer 1993;34:1174.
[27] Kuboyama K, Hara K, Matsushige K. J Appl Phys 1994;33:4135.
[28] Kuboyama K, Hara K, Matsushige K. J Appl Phys 1992;31:L1609.
[29] Akutsu Y, Shimizu S, Kurita K, Yano S. Rep Prog Polym Phys Jpn 1999;42:459.
[30] Ikake H, Hashimoto W, Obara T, Kurita K, Yano S. Kobunshi Ronbunshu (Jpn J Polym Sci Technol) 2000;57:376.
[31] Yano S, Furukawa T, Kodomari M. Rep Prog Polym Phys Jpn 1996; 39:167.
[32] Glatter O. J Appl Crystallogr 1974;7:147.
[33] Schefer DW. Science 1989;243:1023.
[34] Schefer DW, Keefer KD. In: Brinker CJ, Clark DE, Ulrich DR, editors. Better ceramics through chemistry. New York: North Holland; 1984. p. 1.
[35] Ikake H, Fukuda Y, Shimizu S, Kurita K, Yano S. Kobunshi Ronbunshu (Jpn J Polym Sci Technol) 2002;59:608.
[36] Porod G. Kolloid-Z 1951;124:83.
[37] Illers KH. Macromol Chem 1960;38:168.
[38] Woodward AE, Crissman JM, Sauer JA. J Polym Sci 1960;44:23.
[39] Curtis AJ. J Res Natl Bur Stand 1961;65A:185.
[40] Kolarik J, Janacek J. J Polym Sci, Part C 1967;16:441.
[41] Cerrada ML, Benavente R, Perez E, Perena JM. Macromol Chem Phys 2000;201:1858.